Progress in Oceanography 237 (2025) 103515

Contents lists available at ScienceDirect

Progress in Oceanography

journal homepage: www.elsevier.com/locate/pocean

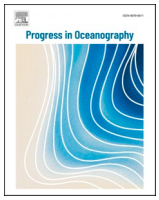

Seasonal variability in surface water pCO_2 and air-sea CO_2 fluxes in the Northwestern Pacific Ocean

Yi Yang, Xianghui Guo *, Dongjian Ci, Yi Xu, Yan Li, Liguo Guo, Minhan Dai

State Key Laboratory of Marine Environmental Science, College of Ocean and Earth Sciences, Xiamen University, Xiamen 361102, China

ARTICLE INFO

Keywords:
Northwestern Pacific Ocean
Partial pressure of CO_2
Air-sea CO_2 fluxes
Seasonal variability
Spatial variability

ABSTRACT

The Northwestern Pacific Ocean is one of the most important carbon sink regions globally. However, spatial variability and seasonal amplitude of surface water CO_2 partial pressure (pCO_2) and air-sea CO_2 fluxes remain unresolved. Surface seawater pCO_2 and auxiliary parameters were investigated in the Northwestern Pacific (10–33°N, 120–158°E) during spring, summer and winter in 2019 and 2020. The air-sea CO_2 fluxes exhibited pronounced seasonal variability, acting as a CO_2 sink of 5.0 ± 4.1 mmol m^{-2} d^{-1} in winter and a CO_2 source of 1.7 ± 1.6 mmol m^{-2} d^{-1} in summer. In summer, the CO_2 source increased with latitude, with the 10–14°N sub-region near equilibrium with the atmosphere (0.6 ± 0.6 mmol m^{-2} d^{-1}) and the 27–33°N sub-region displaying the strongest source (3.6 ± 2.1 mmol m^{-2} d^{-1}). The air-sea CO_2 flux is primarily driven by variability in surface water pCO_2. During summer, surface water pCO_2 increases with latitude (408.4 ± 5.1, 418.2 ± 9.0 and 455.5 ± 12.4 μatm in 10–14°N, 14–27°N and 27–33°N, respectively), showing a "strange" pattern inverse with sea surface temperature. Temperature normalized pCO_2 ($NpCO_2$) also increases with latitude. In winter, surface water pCO_2 generally decreases with latitude (379.4 ± 3.8, 372.9 ± 9.1 and 354.5 ± 3.6 μatm in 10–14°N, 14–27°N and 27–33°N, respectively), but $NpCO_2$ increased with latitude (356.7 ± 7.7, 387.2 ± 13.1 and 434.4 ± 4.4 μatm in 10–14°N, 14–27°N and 27–33°N, respectively). In addition to the dominating temperature effect, different sub-regions have their own unique processes that affect the pCO_2 behavior which in turn influences the air-sea CO_2 fluxes. In the western zone (west of 130°E) of the 10-14°N sub-region, precipitation reduces pCO_2 by 12.4 ± 5.2 μatm in summer and 14.8 ± 4.4 μatm in winter. In the 14-27°N sub-region, the relatively high $NpCO_2$ is primarily driven by evaporation, with elevated salinity increasing surface water $NpCO_2$ by 11.1 ± 12.7 μatm in summer and 7.7 ± 15.3 μatm in winter. The 27–33°N sub-region is located in the Subtropical Mode Water and atmospheric CO_2 intrusion (increasing pCO_2 by 44.2 μatm) also have important contributions to the high $NpCO_2$. Under the context of global warming, the regional changes, such as variations in evaporation and precipitation, have the potential to significantly alter global ocean CO_2 sink/source patterns and weaken the surface ocean's CO_2 sequestration ability.

1. Introduction

The ocean sequesters approximately 25 % of the anthropogenic CO_2 annually (Sabine et al., 2004; Takahashi et al., 2009; Le Quéré et al., 2018), and thus decreases the amount of CO_2 remaining in the atmosphere and mitigates global warming (Sabine et al., 2004). Though the ocean is a vast sink of atmospheric CO_2, the CO_2 exchange between the ocean and the atmosphere varies considerably over both space and time (Takahashi et al., 2002, 2009; Iida et al., 2015). However, significant uncertainties remain concerning the magnitude of these variations in air-sea CO_2 fluxes in certain regions, such as the Intertropical Convergence Zone and mode water areas, due mainly to the lack of understanding regarding the mechanisms controlling the spatiotemporal variations of CO_2 partial pressure (pCO_2) of surface water (Takahashi et al., 2003; Andersson et al., 2013).

The Northwestern Pacific Ocean from 10 to 35°N acts as a net sink for atmospheric CO_2 (Ayers and Lozier, 2012; Wanninkhof et al., 2013; Iida et al., 2015; Fay et al., 2021). Studies have investigated the seasonal, inter-annual and decadal variations in surface water pCO_2 and air-sea CO_2 fluxes in the Northwestern Pacific (Takahashi et al., 2002, 2009; Gruber et al., 2009; Ishii et al., 2014). Surface water pCO_2 exhibits a general seasonal pattern of higher pCO_2 in summer and lower pCO_2 in

* Corresponding author.
E-mail address: xhguo@xmu.edu.cn (X. Guo).

https://doi.org/10.1016/j.pocean.2025.103515
Received 6 July 2024; Received in revised form 2 June 2025; Accepted 4 June 2025
Available online 16 June 2025

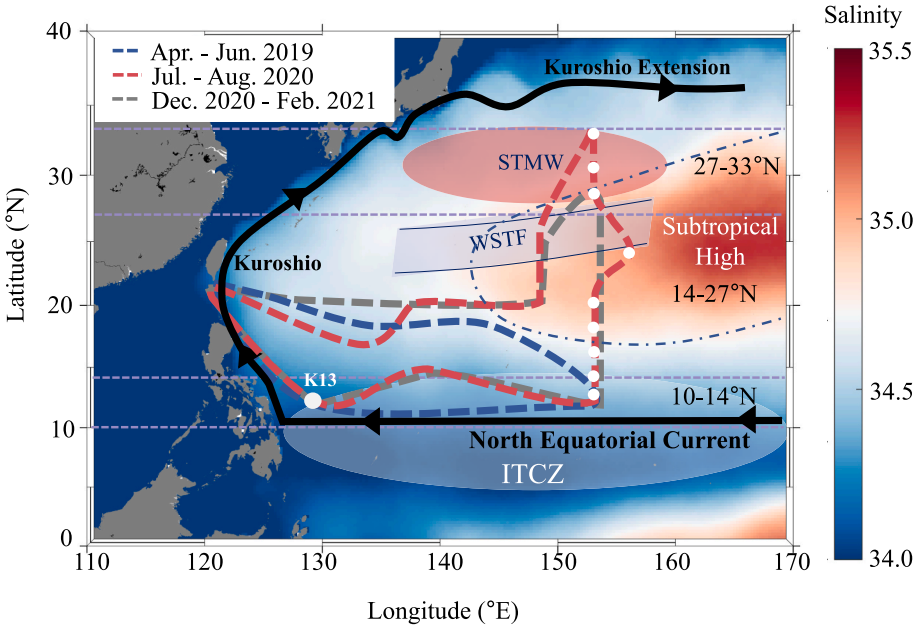

Fig. 1. Map of the Northwestern Pacific with the major surface currents and the cruise tracks (thick dashed lines). The white circle marks station K13 visited during the cruises. Subtropical Mode Water (STMW) is also shown. Blue shading denotes the Western Subtropical Front (WSTF) (revised from Oka and Qiu, 2012). ITCZ is the Intertropical Convergence Zone. The area enclosed by a dash-dot curve is the North Pacific Subtropical High. Colors superimposed on the map represent annual mean sea surface salinity (SSS) in 2020 acquired from the Copernicus Marine Environment Monitoring Services (http://marine.copernicus.eu). The three sub-regions are indicated with thin dotted lines. The white dotes in the eastern section are the sampling stations during the summer cruise and the data are shown in Fig. 8.

winter. Seasonally, this region varies between a sink in winter and a source in summer (Ogawa et al., 2006; Takahashi et al., 2009). Temperature is an important factor driving the spatiotemporal variability of surface water pCO_2 in the Northwestern Pacific, but it is not the sole major factor driving surface water pCO_2 values. Other processes, such as water mixing, biological processes, air-sea exchange, and local precipitation or evaporation, etc., may also play important roles (Ayers and Lozier, 2012). However, how much these processes or factors regulate the surface water pCO_2 and the air-sea CO_2 fluxes is still unknown.

Within the Northwestern Pacific Ocean, there are many water masses and fronts, such as the North Equatorial Current, the Western Subtropical Front (WSTF), Subtropical Mode Water (STMW), the Kuroshio and the Kuroshio Extension (Fig. 1). Additionally, the low latitude zone of the Northwestern Pacific Ocean is located in the Intertropical Convergence Zone (ITCZ), where precipitation dominates (Byrne et al., 2018). The water masses and fronts might have different impacts on the spatiotemporal variability of the surface water pCO_2, or different factors or processes might dominate in different water masses or sub-regions. However, how the sharp spatial temperature variability at the front, the Subtropical High induced strong evaporation, the strong precipitation in the ITCZ, etc., influence surface water pCO_2 is still to be revealed.

In this study we present the seasonal and spatial variability of the surface water pCO_2 and air-sea CO_2 fluxes, based on a dataset of surface water pCO_2 and auxiliary parameters collected during three cruises conducted during spring, summer and winter in 2019–2020, and identify the factors controlling surface water pCO_2 in different sub-regions of the Northwestern Pacific Ocean. Additionally, the influences of precipitation/evaporation and horizontal advections on surface water pCO_2 will be quantified.

2. Materials and methods

2.1. Study area

The study area spans 10–33°N latitude and 120–158 °E longitude in the Northwestern Pacific Ocean (Fig. 1). The primary currents in the study area include the western sector of the North Equatorial Current, the Kuroshio and the Kuroshio Extension. The currents compose the southern, western and northern boundary of the region studied.

The study area is affected by the Western Pacific Warm Pool, and sea surface temperatures (SSTs) are high (> 28 ℃). Subtropical Mode Water (STMW) is located from 27 to 33°N, in the northern zone of the study area. Such mode water with low potential vorticity forces the upper pycnocline to shoal southward and forms the Western Subtropical Front (WSTF) at depths of 0–200 m (Uda and Hasunuma, 1969). In the center of the study area, net evaporation dominates under the descending branches of the Hadley circulation cell, and sea surface salinity (SSS) reaches a maximum (>35) at 20–28°N because of the influence of the North Pacific Subtropical High. The low latitude zone is located within the ITCZ seasonally, which is a precipitation-dominated zone characterized by low SSS (<34.2) with a strong halocline beneath. Between the surface water and the thermocline, there is a barrier layer, so that warm and fresher water is above the warm and salty water (Cravatte et al., 2009).

The study area is characterized by oligotrophic water and very low primary production (Dai et al., 2023). The strong stratification restricts vertical mixing and inputs of nutrient-replete deep water into the surface water (Letscher et al., 2016), which limits primary production (Dai et al., 2023). This also further exacerbates the accumulation of CO_2 in surface water and hinders its downward transport.

We divide the study area into three sub-regions: (1) 10–14°N, (2) 14–27°N, and (3) 27–33°N, according to the different characteristics of each area in the Northwestern Pacific Ocean. The sub-region (1) 10–14°N includes part of the ITCZ zone; the sub-region (2) 14–27°N includes the WSTF; the sub-region (3) 27–33°N is located in the STMW. Part of the sub-regions (2) 14–27°N and (3) 27-33°N are under the influence of the North Pacific Subtropical High (Fig. 1).

2.2. Sampling, analysis and data processing

2.2.1. Cruises and data collection

Data were collected onboard the R/V Tan Kah Kee (Jiageng) during

three cruises conducted from April 25–June 13 of 2019, July 3–August 23 of 2020 and December 23 of 2020–February 13 of 2021 in 10–33°N and 120–158 °E in the Northwestern Pacific Ocean. The track of the spring cruise was within the 10–14°N and 14–27°N sub-regions, and the summer and winter cruises covered all the three sub-regions (Fig. 1).

SST, SSS and pCO_2 of surface water and atmosphere were measured continuously with an underway system. The measurement and data processing methods followed those of Pierrot et al. (2009), and are briefly described here.

Surface water pCO_2 was measured using an air–water equilibrator and laser-based Cavity Ring-Down Spectroscopy (Picarro Model G2301) integrated into a GO-8050 underway system (General Oceanics). The details of the underway system were described in Li et al. (2020). Surface water was continuously pumped from ~ 5 m depth and the CO_2 mole fraction (xCO_2) was determined after air–water equilibration. xCO_2 in the atmosphere was also determined every 1–1.5 h. The intake for the air samples was installed at the bow ~ 10 m above the sea surface to avoid contamination from the ship. SST and SSS were measured with a Seabird SBE 21 system. CO_2 standards with xCO_2 values of 201, 396, 592 and 798 ppm, provided by National Research Center for Certified Reference Materials of China, were used to calibrate the system every eight hours. The overall uncertainty of the underway xCO_2 measurement system is less than ± 1 %.

The barometric pressure and wind speeds were measured continuously with a barometer (Model BARO-1, Vaisala) and WINDCAP ultrasonic wind sensor (Model WMT700, Vaisala) integrated in a Maritime Observation System (Model AWS430, Vaisala). The sensors were ~ 10 m above sea surface. Precision of the barometric pressure and wind speed is ± 3 hPa and ± 0.2 m s^{-1}, respectively.

Water pCO_2 at the temperature in the equilibrator (pCO_2^{Eq}) was calculated from the xCO_2 in the equilibrator and the pressure in the equilibrator (P_{Eq}) after correction for the vapor pressure (P_{H2O}) of water at 100 % relative humidity (Weiss and Price, 1980):

$$pCO_2^{Eq} = \left(P_{Eq} - P_{H_2O}\right) \times xCO_2 \quad (1)$$

Atmospheric pCO_2 was calculated similarly using xCO_2 in the air and the barometric pressure using a formula similar to Formula (1).

Water pCO_2^{Eq} obtained from Formula (1) was corrected to surface water pCO_2 at *in situ* temperature (*in situ* pCO_2, or pCO_2 hereafter) using the empirical formula of Takahashi et al. (1993), where t is temperature in the equilibrator in °C, and SST is the sea surface temperature in °C.

$$\text{in situ } pCO_2 = pCO_2^{Eq} \times \exp((\text{SST-t}) \times 0.0423) \quad (2)$$

Net air-sea CO_2 flux (CO_2 flux or FCO_2 hereafter) between the surface water and the atmosphere was calculated using the following formula:

$$FCO_2 = k \times s \times \Delta pCO_2 \quad (3)$$

where s is the solubility of CO_2 (Weiss, 1974); ΔpCO_2 is the pCO_2 difference between the surface water and the atmosphere; and k is the air-sea CO_2 transfer velocity. k was parameterized using the empirical function of k with wind speed at 10 m above sea surface of Sweeney et al. (2007).

During the summer and winter cruises, surface water was sampled for dissolved inorganic carbon (DIC) and total alkalinity (TA) from the underway system every three hours. We collected totally 201 and 174 underway DIC/TA samples during the summer and winter cruises, respectively. During the spring cruise, surface water DIC/TA samples were collected at 16 stations with 12 L Niskin bottles attached to a CTD rosette (Seabird 911 plus). The sampling sites are shown in Fig. S1. Following the procedure recommended by Dickson et al. (2007), water samples for DIC and TA were collected and stored in 250 mL borosilicate glass bottles with ground glass stoppers and poisoned with 250 μL of saturated $HgCl_2$ solution after removing 2.5 mL of water. The samples were preserved at room temperature in the dark until measurement. DIC was measured using an infrared CO_2 detector-based DIC analyzer (AS-C3, Apollo SciTech Inc.), and TA was determined at 25.0 °C with Gran titration method using a TA titrator (AS-ALK2, Apollo SciTech Inc.). Precision of DIC and TA measurements was ± 0.1 % (Cai et al., 2004). Certified reference materials from Dr. Andrew G. Dickson's Laboratory (Scripps Institute of Oceanography) were used to calibrate the DIC and TA measurements to an accuracy of ± 2 μmol kg^{-1}.

The measured underway DIC and TA data were two-dimensionally interpolated to get a spatial resolution of ~ 0.005° × 0.005° to calculate the influence of variabilities of DIC and TA on surface water pCO_2. The interpolation method is presented in the supplementary materials (S1). For TA: mean absolute error (MAE) = 5.6 μmol kg^{-1}, root mean square error (RMSE) = 7.6 μmol kg^{-1}, relative error (RE) = 0.24 %. For DIC: MAE = 4.0 μmol kg^{-1}, RMSE = 5.4 μmol kg^{-1}, RE = 0.21 %. The validations of the interpolated TA and DIC are shown in Fig. S2. The pCO_2 uncertainties due to the RMSEs of interpreted DIC and TA were 10.1 and −12.1 μatm, respectively, according to Formula 5. The comparisons of the calculated pCO_2 from interpolated DIC and TA with underway measured pCO_2 show that the average, maximum and minimum differences were 11.8 ± 7.5, 33.0 and 0.0 μatm, respectively, for the summer cruise, and 3.9 ± 3.1, 19.5 and 0.0 μatm, respectively, for the winter cruise. The point-to-point comparisons of the calculated and measured pCO_2 are shown in Fig. S3.

2.2.2. Calculations of influences of processes or factors on surface water pCO_2

2.2.2.1. Influences of different factors on the seasonal variability of surface water pCO_2.

To determine the influences of different factors on the surface water pCO_2 seasonal variability, we conducted a decomposition of pCO_2 variations into their driving components, namely temperature (T), salinity (S), DIC and TA, thereby neglecting the very small contributions arising from variations in nutrients and other minor drivers. We used two methods to calculate the influences of different parameters on the seasonal variations of the surface water pCO_2; one is for DIC and TA (Formula 5), and the other is for salinity-normalized DIC and TA (sDIC and sTA) (Formula 6).

Considering only the first-order terms a Taylor expansion gives, for any change in pCO_2, that is, δpCO_2,

$$\delta pCO_2 = \left(\frac{\partial pCO_2}{\partial T}\right) \times \delta T + \left(\frac{\partial pCO_2}{\partial DIC}\right) \times \delta DIC + \left(\frac{\partial pCO_2}{\partial TA}\right) \times \delta TA + \left(\frac{\partial pCO_2}{\partial S}\right) \times \delta S \quad (5)$$

Surface water pCO_2 normalized to a constant temperature of 27°C (average SST of the three cruises), $NpCO_2$, was calculated following Takahashi et al. (2002):

$$NpCO_2 = pCO_2 \times \exp((27 - SST) \times 0.0423) \quad (4)$$

where δ denotes deviation of a certain parameter from the annual average (with the assumption that δ is small relative to the value of the parameter). The DIC and TA data are from Iida et al. (2021).

Since freshwater input to or evaporation from the surface ocean

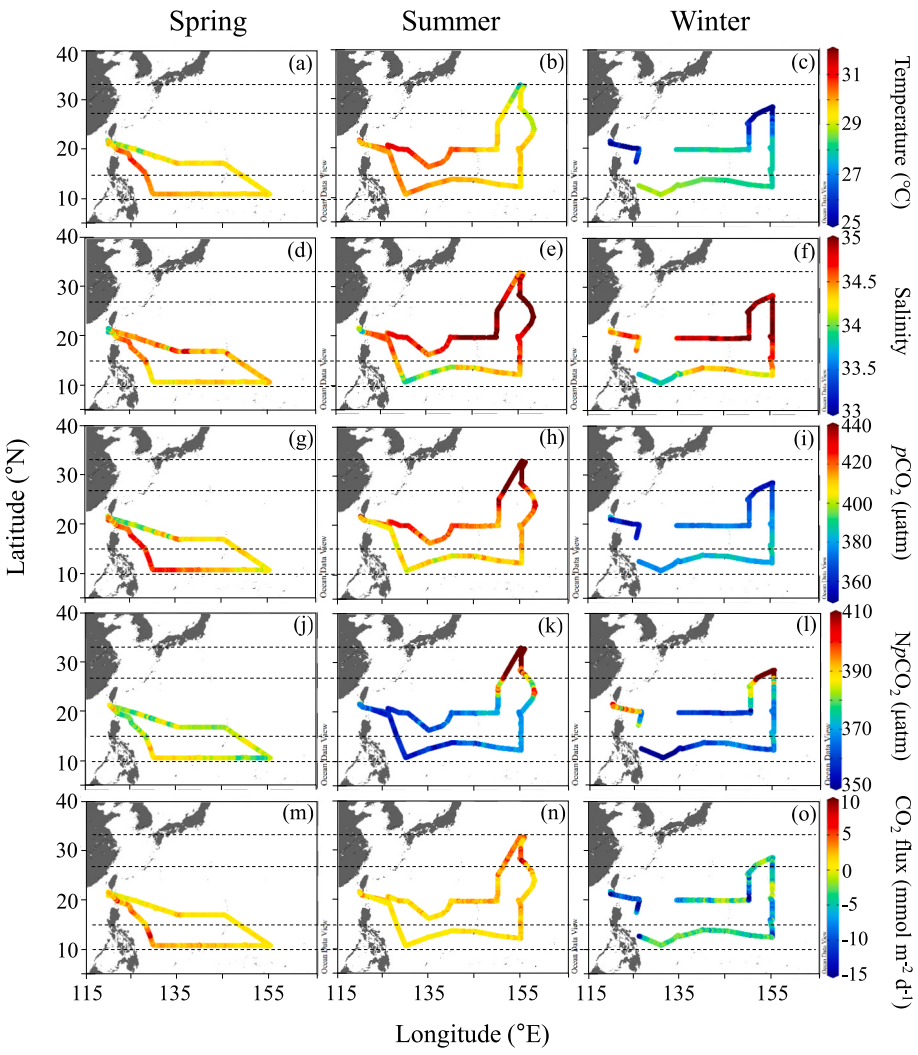

Fig. 2. Distributions of sea surface temperature, sea surface salinity, surface water pCO_2 (pCO_2), pCO_2 normalized to 27 °C ($NpCO_2$) and air-sea CO_2 flux (CO_2 flux) in the Northwestern Pacific during the cruises in spring (a, d, g, j and m), summer (b, e, h, k and n) and winter (c, f, i, l and o). The three sub-regions are indicated with dotted lines.

affects not only salinity but also DIC and TA, it is often more insightful to combine all terms affected by freshwater fluxes into one, leaving only the seasonal changes in sDIC or sTA. sDIC and sTA are given by sDIC = DIC × S_0/S and sTA = TA × S_0/S, with S_0 representing the salinity at which the normalization was made, which here is the annual average salinity.

The partial derivatives with regard to any of the factors (δpCO_2) can be estimated from the pCO_2 sensitivities, γ (Sarmiento and Gruber, 2006), and inserting these sensitivities replacing δ with the seasonal difference.

$$\delta pCO_2 = \frac{\partial pCO_2}{\partial T} \times \delta T + \gamma_{DIC} \times \frac{pCO_2}{DIC} \times \frac{S_0}{S} \times \delta sDIC + \gamma_{TA} \times \frac{pCO_2}{TA} \times \frac{S_0}{S} \times \delta sTA + \gamma_S \times \frac{pCO_2}{S} \times \frac{S_0}{S} \times \delta S \quad (6)$$

where γ_{DIC}, γ_{TA} and γ_S describe the dimensionless surface water pCO_2 sensitivities to DIC, TA and salinity, respectively. γ_{DIC} usually refers to the Revelle factor (RF); γ_{TA} usually refers to the TA factor and γ_S refers to the salinity factor. δ indicates the change of the parameter.

The Revelle factor and TA factor were calculated using the CO2SYS program (van Heuven et al., 2011) with DIC and TA as input parameters. CO_2 dissociation coefficients were from Mehrbach et al. (1973) refitted by Dickson and Millero (1987). The sulfate dissociation constant was from Dickson. (1990). As the Revelle factor and TA factor are close in value but opposite in sign, changes in pCO_2 affected by DIC and TA show similar magnitudes, but in opposing directions (Takahashi et al., 1993). We use 1.6 as the salinity factor following Sarmiento and Gruber (2006). The DIC and TA data used in Formula (6) are the collected data during the cruises.

2.2.2.2. Influence of air-sea CO_2 exchange. Air-sea CO_2 exchange affects DIC but TA remains invariant. Therefore, the DIC change due to air-sea CO_2 exchange ($\delta DIC^{Air\text{-}sea}$) was calculated from FCO_2, mixed layer depth (H) and density (ρ), and then converted to the pCO_2 change ($\delta pCO_2^{Air\text{-}sea}$):

$$\delta DIC^{Air\text{-}sea} = FCO_2 / (\rho \times H) \quad (7)$$

$$\delta pCO_2{}^{Air\text{-}sea} = \delta DIC^{Air\text{-}sea} \times \frac{\partial pCO_2}{\partial DIC} \quad (8)$$

Where the $\frac{\partial pCO_2}{\partial DIC}$ term was given by:

$$\frac{\partial pCO_2}{\partial DIC} = \frac{pCO_2}{DIC} \times RF \quad (9)$$

The air-sea CO_2 flux data are sourced from Iida et al. (2021) and obtained from the Japan Meteorological Agency's website (https://www.jma.go.jp/jma/indexe.html). The mixed layer depth data were from de

Boyer Montégut et al. (2004), which were calculated from the combination of a variable threshold on density profiles and a 0.2 °C threshold on temperature profiles.

2.2.2.3. Influence of advections. The introduction of water masses with distinct DIC and TA plays a key role in modulating surface water pCO_2. When water with different DIC and TA is advected into a region, the resulting changes in DIC/TA ratio alters the CO_2 dynamics, thereby influencing pCO_2. Therefore, the relative variations in DIC and TA are critical in driving the net change in pCO_2 through both Ekman transport and geostrophic convergence.

Horizontal Ekman convergence influences DIC and TA through water masses exchange, and thus impacts surface water pCO_2. The impact of horizontal Ekman convergence on pCO_2 (δpCO_2^{Ek}) was calculated as follows (Gent and McWilliams, 1990; Large et al., 1994; Williams and Follows, 1998):

$$\delta pCO_2^{Ek} = -\nabla(u_{Ek} + vEk)\cdot DIC \cdot \frac{\partial pCO_2}{\partial DIC} - \nabla(u_{Ek} + vEk)\cdot TA\cdot\frac{\partial pCO_2}{\partial TA} \quad (10)$$

where $u_{Ek} = \tau_y/\rho f D$ and $v_{Ek} = -\tau_x/\rho f D$ in $m^2\ s^{-1}$; ρ is density; f is the Coriolis parameter; D is the Ekman depth; τ is the wind stress. The Ekman depth was calculated as $D = \frac{4.3\times U_{10}}{\sqrt{\sin\varphi}}$, U_{10} is the monthly average wind speed at 10 m above sea level ($m\ s^{-1}$), and φ is the latitude (Large and Pond, 1981). Wind stress data were from a scatterometer and modeling, conducted using E.U. Copernicus Marine Service Information (https://doi.org/10.48670/moi-00181).

The horizontal geostrophic convergence also influences DIC and TA through water masses mixing and thus influences surface water pCO_2 ($\delta pCO_2^{Ge\circ}$), which was calculated as follows (Gent and McWilliams, 1990; Large et al., 1994):

$$\delta pCO_2^{Geo} = -\nabla u_{Geo}\cdot DIC \cdot\frac{\partial pCO_2}{\partial DIC} - \nabla u_{Geo}\cdot TA\cdot\frac{\partial pCO_2}{\partial TA} \quad (11)$$

where u_{Geo} is the monthly climatological geostrophic velocity. Geostrophic velocity data were from field and satellite observations, conducted using E.U. Copernicus Marine Service Information (https://doi.org/10.48670/moi-00052). For the calculations of impacts of Ekman and geostrophic convergences (Formulae (10) and (11)), the DIC and TA data are from Iida et al. (2021).

2.2.2.4. Influences of evaporation or precipitation. When water is evaporated, solutes are concentrated and both DIC and TA concentrations rise in direct proportion to salinity. The increasing DIC concentration increases pCO_2, while the increasing TA leads to a pCO_2 decrease. However, determination of the actual increase in surface water pCO_2 is complicated by the effects of the salinity change on the solubility of CO_2 and on the apparent dissociation coefficients of carbonic acid in seawater. We cannot simply consider the salinity sensitivity of surface water pCO_2, because this sensitivity only takes into account the impact of salinity on the dissociation coefficients of carbonic acid, but disregards the facts of DIC and TA change. We thus estimated the total change in surface water pCO_2 that resulted from precipitation or evaporation ($\delta pCO_2^{E/P}$) by considering the total derivative of pCO_2 with regard to changes in salinity (S), DIC, and TA, while keeping temperature invariant:

$$\delta pCO_2^{P/E} = \delta S \times \frac{\partial pCO_2}{\partial S}\Big|_{DIC,\ TA=\ const} + \delta DIC \times \frac{\partial pCO_2}{\partial DIC}\Big|_{S,\ TA=\ const} + \delta TA \times \frac{\partial pCO_2}{\partial TA}\Big|_{S,\ DIC=\ const} \quad (12)$$

where δDIC and δTA are the salinity change-induced changes in DIC and TA. We assumed that these latter two changes are proportional to the salinity changes, δS, with the proportionality given by the respective average concentrations, and obtained by:

$$\delta pCO_2^{P/E} = \delta S \times \frac{pCO_2}{S} \times (\gamma_S + \gamma_{DIC} + \gamma_{TA}) \quad (13)$$

Here, we used the annual averages of surface water pCO_2 and salinity in the study area in the calculation. 1.0 was used for γ_S; γ_{DIC} and γ_{TA} were calculated following Sarmiento and Gruber (2006) which were calculated from TA and DIC in the cruise track. The DIC and TA data used in Formulae (12) and (13) are the collected data during the cruises.

3. Results

3.1. Hydrological setting

In spring, SSTs in the southern transect (11–15.5°N, 29.7–31.0 °C) was relatively higher than the northern transect (17.2–21.0°N, 28.0–29.5 °C). The highest SST (31.0 °C) during the cruise was in the western zone (west of 130 °E) of the southern transect, and the lowest SST was in the western zone (west of 130 °E) of the northern transect (east of the Luzon Strait) (Fig. 2a). In summer, the SSTs exhibited distinct meridional and zonal variability. SSTs were generally higher in the western zone (west of 145°E) (30.3 ± 0.4 °C) than in the eastern zone (29.6 ± 0.3 °C) in the 10–14°N and 14–27°N sub-regions. The minimum SSTs (29.0 ± 0.4 °C) were observed in the 27–33°N sub-region (Fig. 2b). In winter, relatively higher SSTs (>28 °C) were measured in the west zone of the 10–14°N sub-region and lower SSTs (25.4 ± 0.8 °C) were in the northern sub-region (27–33°N) (Fig. 2c). Additionally, low SSTs (25.4 ± 0.8 °C) were also observed in the western zone (west of 125 °E) of the 20–21.5°N transect (east of the Luzon Strait) (Fig. 2c), which might be attributed to local cooling (cold front).

Generally, SSS showed relatively low values in the sub-region from 10 to 14°N and high values in the sub-regions from 14 to 27°N and from 27 to 33°N (Fig. 2d-f). The spring cruise surveyed the two lowest latitude sub-regions only, and SSS ranged from 33.5 to 34.9. In summer and winter, the spatial distribution patterns of SSS were similar, and SSS was low (<34.5) in the western zone (west of 140 °E) of the 10–14°N sub-region and high (>35) at 20-28°N.

In addition to the large spatial variability, both SST and SSS showed large seasonal variations. SST was highest (27.6–31.5 °C) in summer and lowest (22.3–28.7 °C) in winter (Fig. 2a-c). The magnitude of seasonal amplitude of SST increased northward, from ~ 1 °C in the sub-region from 10 to 14°N to ~ 5 °C in the sub-region from 27 to 33°N. Average SST over the entire surveyed area was 27.3 ± 1.6 °C in winter and 29.9 ± 0.6 °C in summer. As only the two low latitude sub-regions were surveyed in spring, the spring average SST (29.6 ± 0.5 °C) was only slightly lower than that in summer.

The seasonal variation of SSS was generally not as pronounced as that of SST. The most distinct characteristic was that SSS in the western zone (west of 140 °E) of the 10-14°N sub-region was relatively low (<34.0) in summer and winter compared to in spring (>34.2). This might be attributed to the seasonal variability of the ITCZ. The ITCZ influences SSS primarily by increasing precipitation, which adds freshwater and dilutes the seawater, leading to lower salinity. It also reduces evaporation due to high cloud cover and frequent rainfall, preventing salinity from rising. In summer and winter, the western zone (west of 140 °E) of the 10–14°N sub-region is strongly influenced by the ITCZ, while it's less influenced by the ITCZ in spring according to salinity distributions. In the sub-region from 10 to 14°N, average SSS was 34.3 ± 0.1 in spring, 34.2 ± 0.2 in summer and 34.1 ± 0.2 in winter. Average SSS was 34.8 ± 0.3 in summer and 34.8 ± 0.2 in winter in the sub-region from 14 to 27°N, and 34.8 ± 0.2 in summer and 34.8 ± 0.1 in winter in the sub-region from 27 to 33°N.

3.2. Spatial and seasonal variability of pCO_2

The observed average atmospheric xCO_2 over the study area during

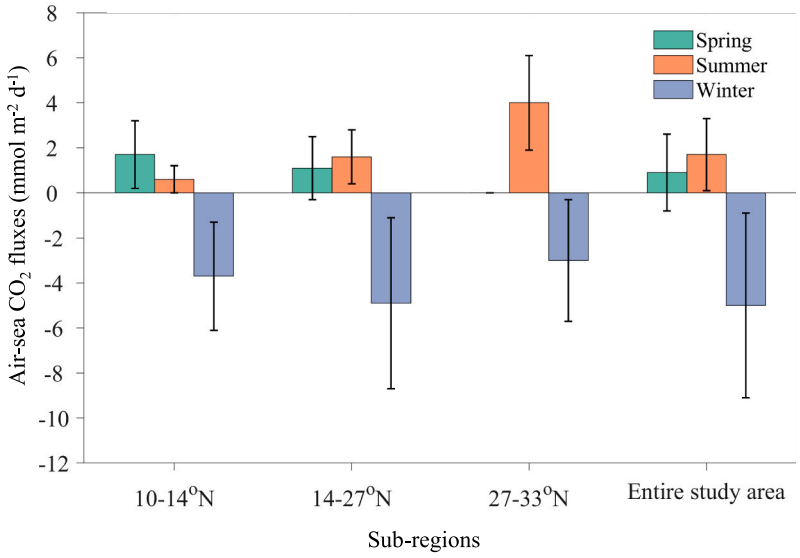

Fig. 3. Regional average sea-air CO_2 fluxes in the Northwestern Pacific Ocean during the three cruises.

the three cruises was 413.5 ± 0.7 ppm in spring, 416.6 ± 2.0 ppm in summer and 417.4 ± 2.7 ppm in winter. The xCO_2 observed during the cruises was generally consistent with but slightly higher than the time-series observations at stations in Guam (data not shown) and Hawaii (Fig. S4). This may be due to the fact that our study area is closer to the eastern Asia, which may have more influences by human activities. Additionally, the observed atmospheric pCO_2 during the cruises showed a slight variation, with 395.0 ± 1.1 μatm and 396.3 ± 1.7 μatm in spring and summer, and 400.5 ± 2.4 μatm in winter.

Surface water pCO_2 (or pCO_2 hereafter) showed large spatial and seasonal variability. Spatially, surface water pCO_2 exhibited strong latitudinal gradients in both summer and winter. In summer, surface water pCO_2 increased northward (Fig. 2h). Average surface water pCO_2 in the three sub-regions from south to north was 408.4 ± 5.1, 418.2 ± 9.0 and 455.5 ± 12.4 μatm, respectively. In winter, the spatial pattern reversed, and surface water pCO_2 decreased northward (Fig. 2i). Average pCO_2 in winter in the three sub-regions from south to north was 379.4 ± 3.8, 372.9 ± 9.1 and 354.5 ± 3.6 μatm, respectively. A detailed description of the pCO_2 in the three seasons is provided in the following paragraphs.

In spring, surface water pCO_2 ranged from 380 to 430 μatm and the spatial pattern followed that of SST (Fig. 2 a, g). The highest value (~ 430 μatm) was observed in the western zone (west of 140 °E) of the southern transect, and the lowest values was in the western zone (west of 130 °E) of the northern transect (east of the Luzon Strait) where surface water pCO_2 was close to atmospheric pCO_2 (~ 395 μatm).

In summer, surface water pCO_2 was generally higher than atmospheric pCO_2 and showed large spatial variability. It generally increased with increasing latitude, from ~ 395 μatm at ~ 11°N to ~ 475 μatm at > 27°N (Fig. 2h). The lowest surface water pCO_2 (408.4 ± 5.1 μatm) was located in western zone (west of 140 °E) of the sub-region from 10 to 14°N (Fig. 2h), in the ITCZ, where the lowest salinity was observed. This will be discussed in the following section.

In winter, surface water pCO_2 was generally lower than the atmospheric pCO_2. Lower values were found in the sub-region from 27 to 33°N, and higher values in the lower latitude sub-regions (Fig. 2i). In the sub-region from 10 to 14°N, surface water pCO_2 varied slightly from ~ 375 μatm to ~ 390 μatm. Along the 155 °E transect, surface water pCO_2 was relatively higher (~ 385 μatm) south of 14°N and lower (~ 375 μatm) in 14-25°N and reached a minimum of ~ 350 μatm in the sub-region from 27 to 33°N (Fig. 2i).

In addition to the spatial variability, surface water pCO_2 also showed large seasonal variability with higher values (higher than atmospheric pCO_2) in spring and summer and lower values (lower than atmospheric pCO_2) in winter (Fig. 2g-i). Additionally, the seasonal variability of surface water pCO_2 differed among the sub-regions. In the sub-region from 10 to 14°N, the seasonal amplitude of pCO_2 was approximately 30 μatm, and pCO_2 was lowest in winter. In this sub-region, the highest pCO_2 values (413.1 ± 8.1 μatm) were observed in spring, even higher than in summer (408.4 ± 5.1 μatm). The relatively lower surface water pCO_2 in summer than in spring was due mainly to the fact that this sub-region is located in the ITCZ in summer, and precipitation decreased the surface water pCO_2 (see discussion in section 4.3). In the sub-region from 14 to 27°N, the seasonal pattern of surface water pCO_2 generally followed that of SST, with pCO_2 higher during summer (417.9 ± 8.8 μatm), followed by spring (410.2 ± 9.6 μatm), and the lowest in winter (373.6 ± 9.1 μatm). The seasonal amplitude of surface water pCO_2 in this region was approximately 50 μatm, larger than that in the sub-region from 10 to 14°N. The largest seasonal amplitude of surface water pCO_2 (>100 μatm) was observed in the sub-region from 27 to 33°N. In this sub-region, the surface water pCO_2 reached 455.5 ± 12.4 μatm in summer, while it decreased to 354.5 ± 3.6 μatm in winter.

In order to better understand the influence of non-temperature effects, surface water pCO_2 was normalized to 27 °C to get $NpCO_2$ (Fig. 2 j, k, l). In spring, there was a slight change in $NpCO_2$, with an average of 368.0 ± 5.7 μatm over the entire surveyed area (Fig. 2j). In summer, $NpCO_2$ showed large spatial variability. The lowest $NpCO_2$ (359.5 ± 5.8 μatm) was in the west zone (west of 140°E) in the 10–14°N sub-region, and the highest $NpCO_2$ (436.5 ± 14.7 μatm) was in the 27-33°N sub-region (Fig. 2k). In winter, the spatial distribution of $NpCO_2$ was similar to the pattern in summer, increased from 356.7 ± 7.7 μatm in 10-14°N to 387.2 ± 13.1 μatm in 14-27°N and 434.4 ± 4.4 μatm in 27-33°N. In addition, relatively higher $NpCO_2$ (386.9 ± 11.3 μatm) also appeared in the low-salinity western zone (west of 125 °E) of the 20–21.5°N transect (east of the Luzon Strait) (Fig. 2l).

3.3. Air-sea CO_2 fluxes

Air-sea CO_2 fluxes showed strong seasonal variability in all sub-regions, and the seasonal pattern differed among the sub-regions. Generally, the sub-region from 10 to 14°N was a moderate to strong CO_2 sink of 3.7 ± 2.4 mmol m^{-2} d^{-1} in winter, a moderate sink to weak source in spring (average air-sea CO_2 flux was 1.7 ± 1.5 mmol m^{-2} d^{-1}) and at near equilibrium with the atmosphere in summer (average air-sea CO_2 flux was 0.6 ± 0.6 mmol m^{-2} d^{-1}) (Fig. 2 m, n, o and Fig. 3).

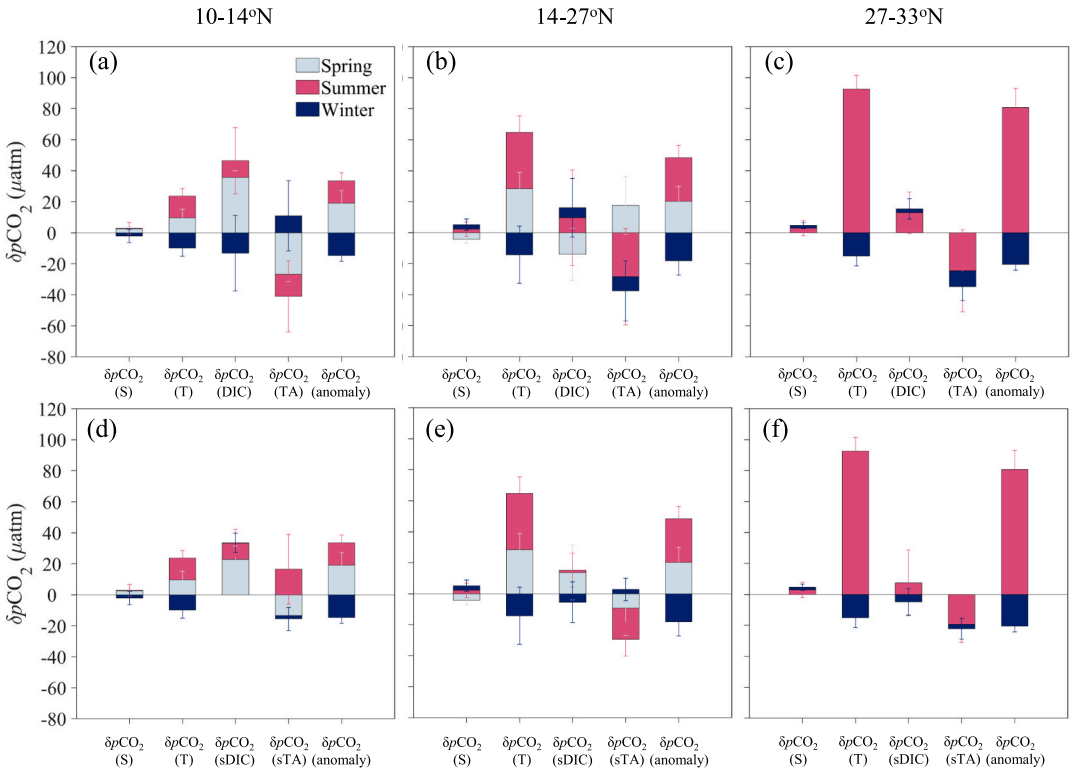

Fig. 4. Effects of seasonal variations in different factors on the surface water pCO_2 (δpCO_2) in each sub-region of the Northwestern Pacific Ocean. δpCO_2(S) indicates the influence of salinity; δpCO_2(T) indicates the influence of temperature; δpCO_2(DIC), δpCO_2(TA), δpCO_2(sDIC) and δpCO_2(sTA) indicate the influence of DIC, TA, sDIC and sTA, respectively; δpCO_2(anomaly) indicates the pCO_2 difference in each season from the annual average. Note that the upper (a-c) and lower (d-f) panels seem similar, and the differences are that the upper panels are calculated based on DIC and TA, while the lower panels are calculated based on salinity-normalized DIC and TA (sDIC and sTA).

The sub-region from 14 to 27°N was a strong sink of 6.0 ± 4.8 mmol m^{-2} d^{-1} in winter, a weak source of 1.1 ± 1.4 mmol m^{-2} d^{-1} in spring, and a weak to moderate source of 1.6 ± 1.2 mmol m^{-2} d^{-1} in summer. The sub-region from 27 to 33°N was a moderate to strong sink of 4.5 ± 3.7 mmol m^{-2} d^{-1} in winter, and a moderate to strong source of 3.6 ± 2.1 mmol m^{-2} d^{-1} in summer (Fig. 2 m, n, o and Fig. 3). Average air-sea CO_2 fluxes over the study area were 1.7 ± 1.6 mmol m^{-2} d^{-1} in summer and −5.0 ± 4.1 mmol m^{-2} d^{-1} in winter; average of summer and winter was −1.7 ± 4.6 mmol m^{-2} d^{-1}.

Studies show similar spatial and temporal distributions of air-sea CO_2 fluxes across the overall range in the Northwestern Pacific. Takahashi et al. (2009) reported annual average air-sea CO_2 flux of about −1.5 mmol m^{-2} d^{-1} in our study area. In northwestern tropical Pacific, Pittman et al. (2022) reported the air-sea CO_2 flux of −0.58 mmol m^{-2} d^{-1} which is consistent with our estimates in the sub-region from 10 to 14°N. In northwestern Pacific subtropical region, the moored time series observation at WHOTS indicates that air-sea CO_2 flux is −0.9 mmol m^{-2} d^{-1} (Sutton et al., 2017), which is slightly lower than our observation. Additionally, based on the dataset of Iida et al. (2020), the annual average air-sea CO_2 flux in in the sub-region from 14 to 27°N is −1.3 mmol m^{-2} d^{-1}, which is also consistent with our observations in this sub-region (−1.1 mmol m^{-2} d^{-1}). In the sub-region from 27 to 33°N, the closest moored time series observations at KEO indicates the air-sea CO_2 flux of −4.0 to −6.6 mmol m^{-2} d^{-1} (Sutton et al., 2017). Gruber et al. (2009) also reported an annual average air-sea CO_2 flux of −4.0 mmol m^{-2} d^{-1} in the Northwestern Pacific. Both of them are consistent with our winter observations.

The comparison of our observation with literature report indicate that our observations have general seasonal representativeness, which is the basis explaining the regulating mechanisms of the surface water pCO_2 using the cruise data. It should be noted that our surveyed area is very limited in the northwestern Pacific compared to the public pCO_2 dataset such as SOCAT, so the air-sea CO_2 flux we reported in this study might be not robust.

4. Discussion

Although atmospheric pCO_2 shows variability, it's much more stable seasonally than the surface water pCO_2. Therefore the seasonal variability of surface water pCO_2 is discussed in this section. We primarily examine the influences of different factors affecting the surface water pCO_2 seasonality (pCO_2 differences between the specific seasons and the annual average, the latter of which is from the dataset of Iida et al. (2020). Special attention will be paid to explain the very high surface water pCO_2 in the sub-region from 27 to 33°N (mode water) in summer, the relatively low pCO_2 in the western zone (west of 140 °E) of the 10–14°N sub-region in summer and winter (ITCZ), and the relatively high pCO_2 in the area influenced by the Subtropical High.

4.1. Effect of different factors on the seasonal variability of surface water pCO_2

In order to reveal the impact of various factors on the surface water pCO_2, we utilized the thermodynamic equations of the carbonate system to calculate the pCO_2 changes with temperature, salinity, DIC (and sDIC) and TA (and sTA) relative to the annual average using formulae 5 and 6. The results are presented in Fig. 4. The main factors controlling the seasonal variability of surface water pCO_2 differed among the three sub-regions.

In the sub-region from 10 to 14°N, the magnitude of the effects of temperature, DIC and TA were generally comparable although the directions were different, while the influence of salinity was negligible (Fig. 4a). The increase of SST in spring and summer increased pCO_2 by 10–14 μatm, and the cooling in winter decreased pCO_2 by 10.0 ± 5.3

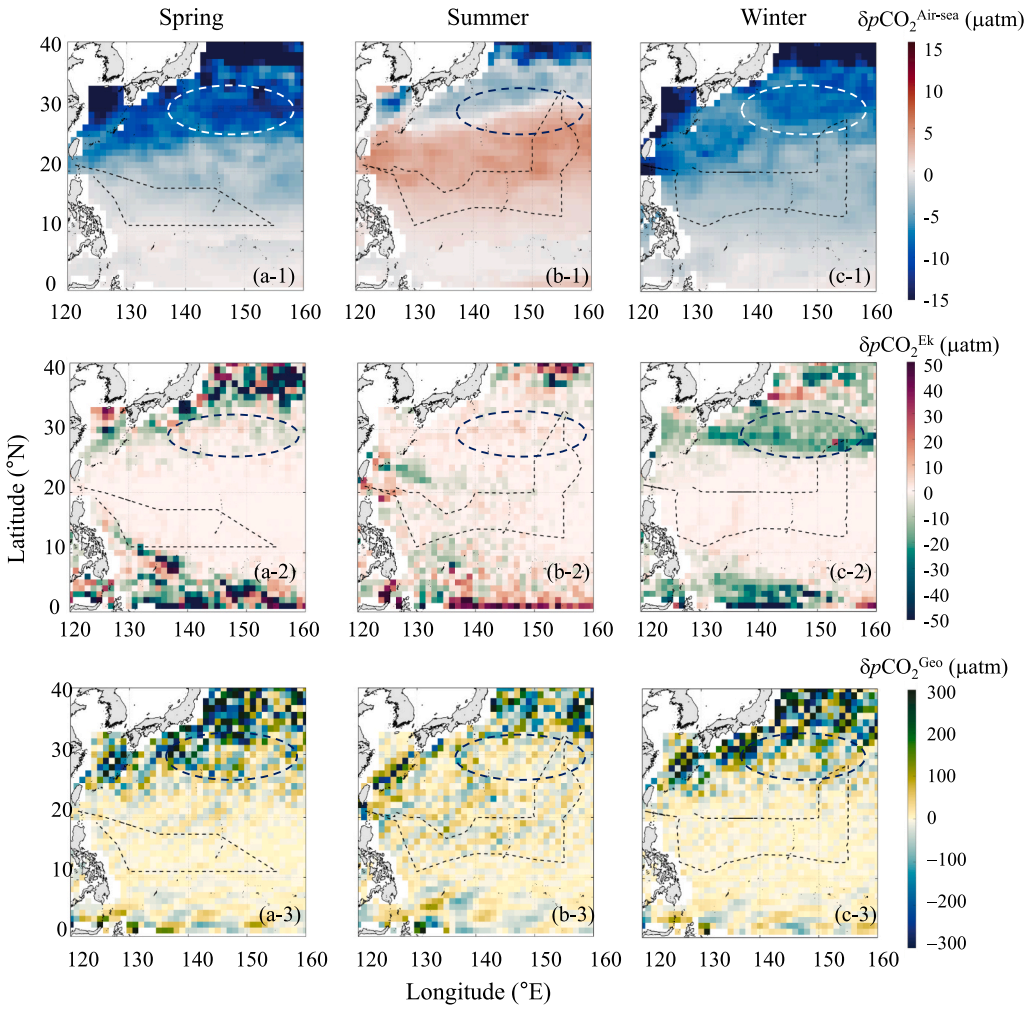

Fig. 5. Influence of air-sea CO_2 exchange ($\delta pCO_2^{Air\text{-}sea}$, a-1 to c-1), horizontal Ekman transport (δpCO_2^{Ek}, a-2 to c-2) and horizontal geostrophic transport (δpCO_2^{Geo}, a-3 to c-3) on surface water pCO_2. The cruise tracks were marked with thin dashed liens. The dashed ellipse encloses the STMW.

μatm. In spring and summer, the effects of DIC and TA variability on surface water pCO_2 almost offset each other, i.e. the effect of elevated DIC increased pCO_2 by 35.8 ± 4.1 and 10.7 ± 21.2 μatm, respectively, while the effect of elevated TA decreased pCO_2 by 26.7 ± 4.7 and 14.3 ± 22.9 μatm, respectively (Fig. 4a). The effects of DIC and TA variability on pCO_2 in winter were −13.1 ± 24.3 and 10.9 ± 22.6 μatm, respectively. When DIC and TA were normalized to the annual average salinity, the sDIC variability increased pCO_2 by 10.4 ± 8.9 and 22.8 ± 8.6 μatm in spring and summer; the effect of sTA variability decreased pCO_2 by 13.4 ± 7.4 μatm in spring and increased pCO_2 by 16.5 ± 22.5 μatm in summer. However, the influences of sDIC and sTA changes were negligible in winter (Fig. 4d).

In the sub-region from 14 to 27°N, SST emerged as the primary determinant of surface water pCO_2, with the ~ 2 °C SST rise during spring and summer leading to a pCO_2 increase of 30–35 μatm. In winter, SST decreased by 1 °C and resulted in a pCO_2 reduction of ~ 15 μatm. The contributions of the variations in DIC and TA also played important roles on the pCO_2 variability. During spring, DIC experienced a decrease of ~ 8 μmol kg^{-1}, resulting in a pCO_2 reduction of ~ 14 μatm. In contrast, the increase in DIC in summer and winter increased pCO_2 by ~ 10 and ~ 7 μatm, respectively. However, there was a TA decrease of ~ 10 μmol kg^{-1} in spring, resulting in a pCO_2 rise of ~ 19 μatm. TA increases of ~ 17 and 6 μmol kg^{-1} during summer and winter led to pCO_2 decreases of ~ 28 and 9 μatm, respectively (Fig. 4b). When DIC and TA were normalized to the annual average salinity during summer and winter, the variation of sDIC remained close to zero, exerting minimal influence on pCO_2. The seasonal variations in sTA during winter were minor, resulting in very limited impact on pCO_2 (Fig. 4e).

In the sub-region from 27 to 33°N, SST was also the dominating factor driving the seasonal fluctuations of surface water pCO_2. During summer, SST rose by 5 °C, resulting in a pCO_2 increase of ~ 95 μatm. In contrast, SST decreased by ~ 1.1 °C in winter, leading to a pCO_2 reduction of ~ 15 μatm. The DIC variability remained near zero during winter, exerting a minor influence on pCO_2. During summer, a DIC increase of ~ 6 μmol kg^{-1} led to a pCO_2 reduction of ~ 13 μatm, and a TA increase of ~ 15 μmol kg^{-1} led to a pCO_2 reduction of ~ 25 μatm (Fig. 4c). Similarity, when DIC and TA were normalized to the annual average salinity, the sDIC anomaly remained near zero during both summer and winter, exerting minor influences on pCO_2. During summer, a sTA increase of ~ 10 μmol kg^{-1} led to a pCO_2 reduction of ~ 19 μatm. Conversely, sTA variability in winter was close to zero, resulting in a negligible effect on pCO_2 (Fig. 4f).

In summary, temperature is an important factor regulating the seasonal variability of surface water pCO_2 and its importance increases with increasing latitude. Additionally, seasonal changes in DIC and TA also play non-negligible roles in the seasonal variability of pCO_2. In the sub-regions from 10 to 14°N from 14 to 27°N, salinity variability also plays a role in regulating the surface water pCO_2, which will be further discussed in section 4.3, taking into account circumstances in the zones of the ITCZ and Subtropical High.

Table 1
Surface water temperature, salinity, pCO_2, $NpCO_2$ (normalized pCO_2 to 27 °C), air-sea CO_2 fluxes (FCO_2), DIC, TA, and salinity-normalized DIC and TA (sDIC and sTA) in the three sub-regions sampled during the cruises.

Sub-region	Season	Temperature (°C)	Salinity	pCO_2 (μatm)	$NpCO_2$ (μatm)	FCO_2 (mmol m^{-2} d^{-1})	DIC (μmol kg^{-1})	TA (μmol kg^{-1})	sDIC (μmol kg^{-1})	sTA (μmol kg^{-1})
10-14°N	Spring	29.7 ± 0.3	34.3 ± 0.1	413.1 ± 8.1	385.0 ± 3.7	1.7 ± 1.5	1943.2 ± 2.1	2262.8 ± 2.6	1978.8 ± 3.5	2304.2 ± 1.4
	Summer	29.9 ± 0.3	34.2 ± 0.2	408.4 ± 5.1	361.6 ± 6.2	0.6 ± 0.6	1929.9 ± 12.0	2254.4 ± 14.6	1975.2 ± 3.9	2307.3 ± 4.3
	Winter	28.5 ± 0.3	34.1 ± 0.2	379.4 ± 3.8	356.7 ± 7.7	−3.7 ± 2.4	1921.1 ± 14.5	2244.1 ± 16.6	1969.7 ± 2.6	2300.9 ± 3.8
14-27°N	Spring	29.6 ± 0.6	34.4 ± 0.2	410.2 ± 9.6	382.9 ± 3.7	1.1 ± 1.4	1950.3 ± 9.2	2273.3 ± 11.5	1976.2 ± 2.7	2302.4 ± 3.3
	Summer	30.1 ± 0.6	34.8 ± 0.3	418.2 ± 9.0	383.3 ± 11.1	1.6 ± 1.2	1958.7 ± 16.6	2294.9 ± 19.8	1971.6 ± 5.5	2310.1 ± 5.7
	Winter	27.1 ± 1.2	34.8 ± 0.2	372.9 ± 9.1	387.2 ± 13.1	−4.9 ± 3.8	1958.2 ± 15.2	2282.9 ± 16.0	1969.4 ± 8.2	2298.2 ± 4.1
27-33°N	Summer	29.0 ± 0.4	34.8 ± 0.2	455.5 ± 12.4	436.5 ± 14.7	4.0 ± 2.1	1987.9 ± 6.9	2297.9 ± 15.5	1990.5 ± 8.1	2309.6 ± 4.6
	Winter	23.2 ± 0.4	34.8 ± 0.1	354.5 ± 3.6	434.4 ± 4.4	−3.0 ± 2.7	1968.9 ± 4.5	2295.9 ± 8.9	1989.4 ± 3.9	2298.9 ± 1.4

4.2. *Very high pCO_2 in the Subtropical Mode Water zone in summer*

Mode waters refer to subsurface oceanic water masses characterized by nearly uniform temperatures, extending a few hundred meters in thickness and spanning several thousand kilometers horizontally (Oka and Qiu, 2012). Subtropical Mode Water (STMW) originates on the warmer side of the western boundary current during late winter due to intense convective mixing within the deep mixed layer (Qiu et al., 2006). By spring, this water is capped by a seasonal pycnocline, maintaining its distinct properties. During summer, the area south of STMW experiences subduction of North Pacific Tropical Water, marked by higher salinity, while the northern region is influenced by the Kuroshio Extension and is characterized by a notable temperature front. Within the STMW, the mixed layer depth tends to remain shallow. The considerable variance in water properties between the north and south of the STMW leads to the retention of surface waters, resulting in an extended residence time for seawater and the preservation of CO_2.

In summer, both pCO_2 and $NpCO_2$ in STMW were highest, along with the lowest SST in the surveyed area. This is inconsistent with the thermodynamics of the CO_2 systems: i.e., water with low SSTs should have low pCO_2. In order to understand this apparently "strange" phenomenon, we quantified the influences of different processes, including air-sea CO_2 exchange, advections (including horizontal Ekman and geostrophic transports, Figs. S5 and S6) and precipitation or evaporation, on the surface water pCO_2.

The results are shown in Fig. 5. We take winter as a reference. From winter to summer, SST increase elevates surface water pCO_2 by 132.0 μatm, while salinity variation has little effect on pCO_2, reducing it by only 2.3 μatm. Additionally, this sub-region is a strong CO_2 sink from October to June and a weak CO_2 source from July to September. The air-sea CO_2 exchange increases the surface water pCO_2 by 44.2 μatm from winter to summer. As the depth of the mixed layer shoals from winter to summer, seawater with high DIC in the subsurface layer has little effect on the surface layer. Therefore, the effect of vertical mixing on pCO_2 is ignored. However, horizontal mixing plays an important role in the seasonal variability of surface water pCO_2. During the transition from winter to summer, Ekman and geostrophic advections decreases pCO_2 by 35.1 μatm and 32.6 μatm, respectively (Fig. 5 b-2 to c-3). Ekman transport is mainly controlled by wind. In the sub-region from 27 to 33°N, wind stress intensity in summer is the lowest, so Ekman transport has the least effect on pCO_2 in summer. In addition, evaporation decreases pCO_2 by 0.6 μatm from winter to summer.

In summary, in the STMW, the temperature rise from winter to summer increases pCO_2 by 132.0 μatm, the salinity variation decreases pCO_2 by 2.3 μatm, and air-sea exchange increases pCO_2 by 44.2 μatm. Ekman and geostrophic advections decrease pCO_2 by 35.1 and 32.6 μatm, and evaporation decreases pCO_2 by 0.6 μatm. The net effects of the above processes and factors increases pCO_2 by 105.7 μatm from winter to summer. In the sub-region from 27 to 33°N, the observed pCO_2 in winter was 354.5 ± 3.6 μatm. Over the period from winter to summer, sea surface pCO_2 increases by 105.7 μatm as calculated above, which would be 460.2 μatm in summer. This value is highly consistent with the observed pCO_2 (455.5 ± 12.4 μatm) during the summer cruise. This consistency indicates that strong change in SST is the primary regulating factor of surface water pCO_2, but air-sea CO_2 exchange and horizontal mixing also play important roles nevertheless in regulating the surface water pCO_2 in the STMW.

Spatially, the three sub-regions have different characteristics, i.e. the

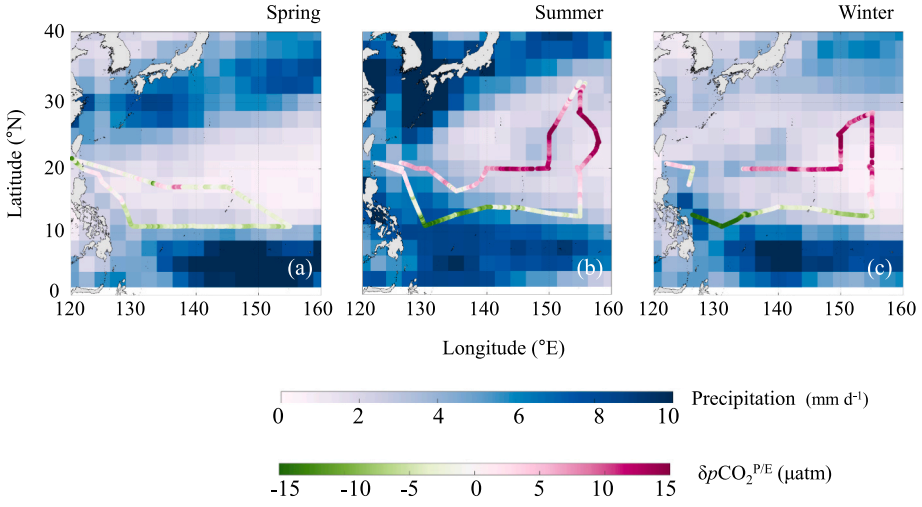

Fig. 6. Influences of evaporation and precipitation on sea surface pCO_2 ($\delta pCO_2^{P/E}$) during the three cruises. The color maps show the monthly average precipitation and the data in the track indicate the $\delta pCO_2^{P/E}$. The monthly average precipitation data are from the National Center for Environmental Information, National Oceanic and Atmospheric Administration (https://www.ncei.noaa.gov).

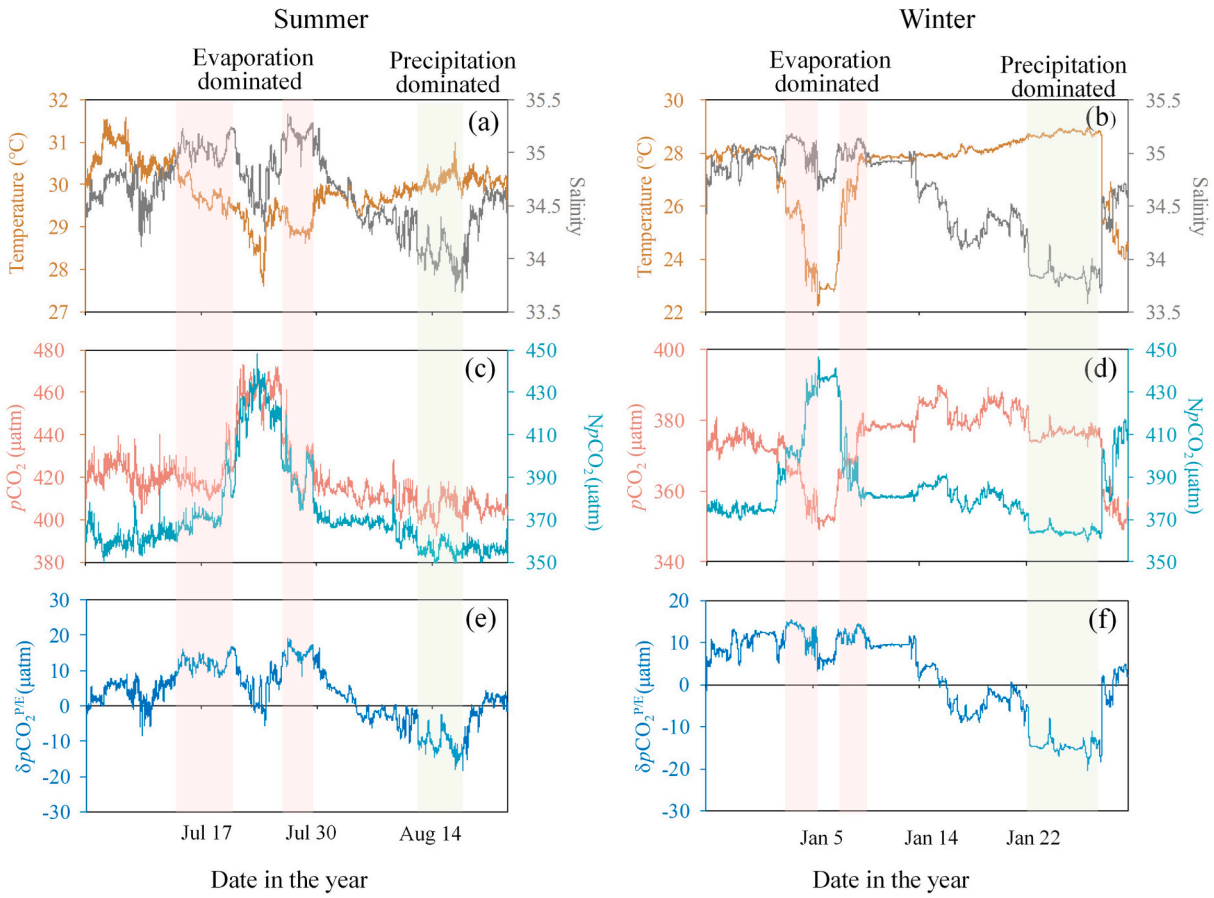

Fig. 7. Distributions of sea surface temperature, salinity, pCO_2, $NpCO_2$ (normalized pCO_2 to 27 °C) and pCO_2 change influenced by precipitation or evaporation ($\delta pCO_2^{P/E}$) in summer and winter along the cruise tracks. The red shaded areas indicate data collected in high salinity (evaporation dominated) zones in the western subtropical front (WSTF); the green shaded area represents data collected in the low salinity (precipitation dominated) zone (Intertropical Convergence Zone, ITCZ).

ITCZ in 10-14°N, the Subtropical High in 14–27°N and the STMW in 27-33°N. In the ITCZ, strong precipitation decreases pCO_2; in the Subtropical High, strong evaporation increases pCO_2; in the STMW, CO_2 sequestration increases pCO_2. Therefore, $NpCO_2$ increases with latitude in both winter and summer (Table 1). If winter is taken as a reference, temperature increase from winter to summer elevates pCO_2 by 132.0 μatm in 27-33°N, 58.4 μatm in 14-27°N and 39.5 μatm in 10-14°N. Therefore, the northward increasing $NpCO_2$ and the temperature variation collectively resulted the "strange" northward increasing pCO_2 pattern in summer.

Furthermore, the extended water retention time within this sub-region also emerges as an important factor contributing to the elevated surface water pCO_2. The prolonged residence time hampers efficient seawater exchange with surrounding regions, impeding the outward transport of the high-CO_2 water mass. Consequently, the surface water pCO_2 in the STMW remains notably higher, amplifying its role as a CO_2 source in summer. Specifically, the CO_2 source in this sub-region (27–33°N) in summer was 2.4 mmol m^{-2} d^{-1} stronger, while the CO_2 sink in winter was 1.9 mmol m^{-2} d^{-1} weaker compared with the sub-region from 14 to 27°N (Table 1).

Studies suggest that mode water plays an important role to the downward transport and storage of anthropogenic CO_2 (Gruber et al., 2019). However, the surface water above STMW in summer has high SSTs. Over long time-scales, the CO_2 source intensity will increase as a result of the surface water pCO_2 increases, and more CO_2 will be released (Fig. S7), thus reducing the carbon sequestration capacity of the mode water.

4.3. *Influence of regional precipitation and evaporation on surface water pCO_2 in the Intertropical Convergence Zone and Subtropical High*

In the low SSS waters of Western Pacific Warm Pool, a barrier layer is often formed within the isothermal layer above the thermocline (Ando and McPhaden, 1997). The formation of a barrier layer can raise SST by preventing colder water under the thermocline from mixing with the warm surface water. It has also been observed that the formation of a barrier layer could reduce surface water DIC owing to the biological uptake that is possibly supported by nitrogen fixation as well as insulation from the DIC-rich water below the thermocline (Ishii et al., 2001). During our cruises, the barrier layer was observed above the thermocline at station K13 (11°N, 130 °E, Fig. S8), which is situated within the precipitation-dominated region.

4.3.1. *Intertropical Convergence Zone: Precipitation dominated zone*

As stated in section 3.1, the west zone (west of 140 °E) of the sub-region from 10 to 14°N is located in a region influenced by the ITCZ (precipitation dominated zone) in summer and winter, but not in spring, which is obvious from the spatial distributions of the monthly average precipitation (Fig. 6). In this sub-region, the spatial trends of surface water pCO_2 and $NpCO_2$ in spring differ from those in summer and winter (Fig. 2 g-l).

Precipitation leads to a reduction in the mixed layer depth and an enhancement of stratification within this particular zone. Precipitation also dilute DIC and TA in proportion to salinity. The decreasing DIC concentration decreases pCO_2, while the decreasing TA leads to a pCO_2 increase. However, determination of the variation in surface water pCO_2 is complicated by the effects of the salinity change on the solubility of

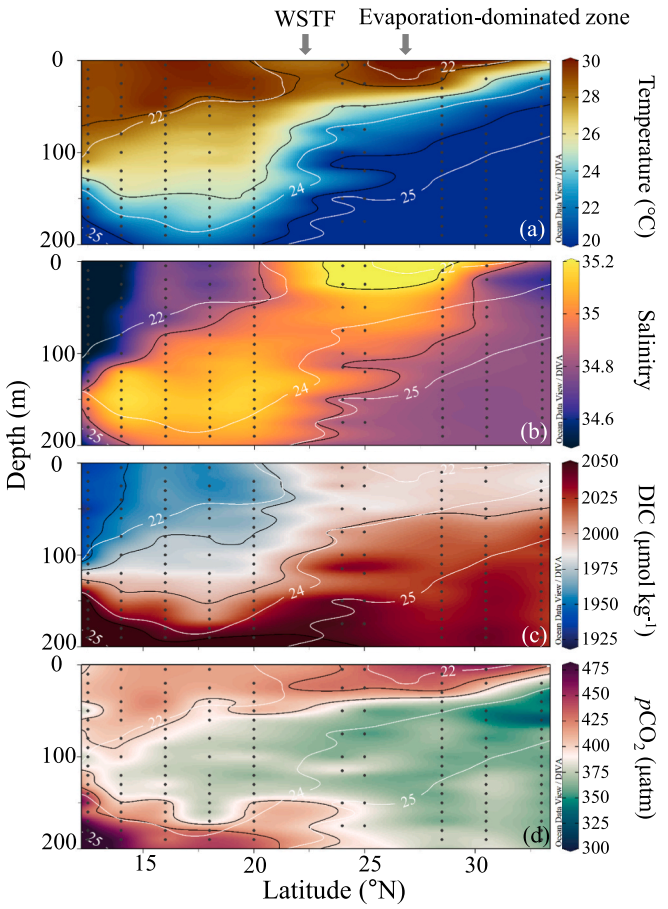

Fig. 8. Latitudinal distributions (12-33°N, 155°E) of surface water temperature, salinity, DIC and pCO_2 during summer cruise. White lines are the isopleths of potential density and black lines are isopleths of the parameters; the black dots indicate the sampling stations and depths. The arrows show the Western Subtropical Front (WSTF) and the evaporation-dominated zone. The sampling stations are shown in Fig. 1 with white dotes.

CO_2 and on the apparent dissociation coefficients of carbonic acid in seawater. We cannot simply consider the salinity sensitivity of surface water pCO_2, because this sensitivity only takes into account the impact of salinity on the dissociation coefficients of carbonic acid, but disregards the facts of DIC and TA change. In order to quantify the effect of rainfall on surface water pCO_2, we only consider the dilution effect of precipitation on salinity, DIC and TA. The results are presented in Fig. 6. The cruise track in spring was not in the ITCZ and the precipitation influenced pCO_2 change ($\delta pCO_2^{P/E}$) was slight (<5 μatm, Fig. 6a), so we only discuss the $\delta pCO_2^{P/E}$ in summer and winter.

In the western zone (west of 140 °E) of the sub-region from 10 to 14°N, precipitation reduces pCO_2 by 10.5 ± 2.9 μatm in summer and 14.7 ± 1.5 μatm in winter (Fig. 6b and c). In summer, the observations show that $NpCO_2$ in the zone experiencing high precipitation was 371.2 ± 3.1 μatm, while the low precipitation zone (east of 140 °E) had a $NpCO_2$ of 383.6 ± 4.2 μatm. The difference, 12.4 ± 5.2 μatm, is consistent with the calculated influence of precipitation on pCO_2 (10.5 ± 2.9 μatm). In winter, the $NpCO_2$ in the high-precipitation region (west of 140 °E) was 364.2 ± 1.4 μatm, and in the low-precipitation region (east of 140 °E) was 379.0 ± 4.2 μatm, with a difference of 14.8 ± 4.4 μatm, which also agrees with the calculated influence of precipitation (14.7 ± 1.5 μatm). The above results suggest that precipitation has an important influence on the surface water pCO_2 in the low latitude sub-region of the Northwestern Pacific Ocean.

4.3.2. North Pacific Subtropical High: Evaporation dominated zone

The Subtropical High is an evaporation-dominated zone experiencing high SSS. Part of the 20–27°N latitude during the summer and winter cruises was in the zone impacted by the Subtropical High. We define salinity > 35.1 as the high-evaporation zone and salinity < 35.1 in the same latitude range as the area beyond the high-evaporation zone. Average SSS in the high-evaporation zone was 35.2 ± 0.1 and 35.1 ± 0.0 in summer and winter, respectively, based on the cruise observations. They were 0.7 and 0.6 higher than the annual average SSS in the Northwestern Pacific (34.5, based on the climatological salinity data in the 10–33°N latitude and 120-160°E longitude from E.U. Copernicus Marine Service Information, https://doi.org/10.48670/moi-00052). The elevated SSS increased the surface water pCO_2 by 15.3 ± 1.0 μatm in summer and 14.3 ± 0.5 μatm in winter (Fig. 6b and c).

This value is roughly the same as half of the amplitude of the annual cycle of δpCO_2 (Fig. 4). The observations showed that the evaporation-dominated area in the northern part of the WSTF exhibits high salinity, which leads to an increase in surface water $NpCO_2$. The observed $NpCO_2$ in the evaporation-dominated zone was 384.9 ± 10.4 μatm in summer and 397.3 ± 8.0 μatm in winter. The $NpCO_2$ in the zone beyond the evaporation-dominated area (the same latitude range beyond the Subtropical High) was 373.8 ± 7.3 μatm in summer and 389.6 ± 13.1 μatm in winter. The differences between the evaporation-dominated and beyond the evaporation-dominated zones are 11.1 ± 12.7 μatm in summer and 7.7 ± 15.3 μatm in winter, and are comparable to the estimates of evaporation influenced pCO_2 change above (15.3 ± 1.0 μatm in summer and 14.3 ± 0.5 μatm in winter). The consistency between observations and estimates supports the strong influence of the evaporation on surface water pCO_2.

Fig. 7 shows the $\delta pCO_2^{P/E}$ together with the surface water temperature, salinity, pCO_2 and $NpCO_2$. In both summer and winter, the evaporation-dominated (high salinity) zones have high $NpCO_2$, and evaporation increases the pCO_2 by 10–20 μatm. Conversely, the precipitation-dominated (low salinity) zone has low $NpCO_2$, and precipitation results in a pCO_2 drawdown of ~ 20 μatm. Overall, distributions of all the parameters matched very well with the estimated $\delta pCO_2^{P/E}$.

Based on the DIC and TA collected underway in the 155°E transect, pCO_2 values within the upper 200 m were calculated with the program CO2SYS. The results show that in the zone affected by strong evaporation, pCO_2 significantly increases, further confirming that evaporation increases surface water pCO_2 (Fig. 8). On the other hand, a significant rise (from south to north) in DIC in the zone north of the WSTF also adds to the relatively high pCO_2. These factors synergistically contribute to the elevated surface water pCO_2 within this evaporation-dominated zone. This study strongly suggests that although temperature and DIC (including the influence of air-sea CO_2 exchange) are crucial factors governing the seasonal variability of the surface water pCO_2 in the Northwestern Pacific, the influences of local precipitation and evaporation should not be ignored.

In the context of global climate change, global warming will increase surface water pCO_2 (Takahashi et al., 2002) and hence might decrease the CO_2 sink ability of the ocean. Simultaneously, global warming has increased dryness, especially in the subtropical regions (Li et al., 2012). Additionally, the ITCZ width is narrowing and the subtropics are widening (Lu et al., 2007; Frierson et al., 2007; Seidel et al., 2008; Lau and Kim, 2015). This means that in the marginal regions of the ITCZ, such as the low latitude zone in our study area, rainfall is weakening, and the area affected by the Subtropical High is increasing and becoming saltier. According to our findings, this scenario will strengthen the CO_2 source in summer and weaken the CO_2 sink in winter if wind speeds have no significant change, thereby also decreasing the ocean's ability to sequester CO_2 from the atmosphere.

5. Concluding remarks

Surface water pCO_2 and air-sea CO_2 fluxes in the Northwestern Pacific Ocean show large spatial and seasonal variations. Additionally, surface water pCO_2 increases with latitude which is contrary to common sense. SST is the most important factor regulating the seasonal variability of the surface water pCO_2 in the sub-regions from 14 to 27°N and 27–32°N, although the seasonal variabilities of DIC and TA also play non-negligible roles in the sub-region from 10 to 14°N. In the Subtropical Mode Water, surface water pCO_2 is up to ~ 440 μatm in summer, which is mainly regulated by SST, air-sea CO_2 exchange and horizontal advections. The mode water strengthens the CO_2 source in summer and weakens the CO_2 sink in winter. In some specific zones, such as the Subtropical High and the ITCZ, evaporation or precipitation also play important role. In the Subtropical High, evaporation increases pCO_2 by 15.3 ± 1.0 μatm in summer and 14.3 ± 0.5 μatm in winter. In the ITCZ, precipitation decreases pCO_2 by 10.5 ± 2.9 μatm in summer and 14.7 ± 1.5 μatm in winter. The very high NpCO_2 in the mode water, the high NpCO_2 in the Subtropical High influenced zone and low NpCO_2 in the ITCZ explained the "strange" pCO_2 spatial distribution, i.e. pCO_2 increase with increasing latitude in summer.

Under the context of global change, global warming may directly reduce oceanic CO_2 sequestration. Furthermore, regional changes regulated by global warming, such as variations in evaporation and precipitation, have the potential to significantly alter global ocean CO_2 sink/source patterns and weaken the surface ocean's CO_2 sequestration ability indirectly, which should be considered when modelling the oceanic carbon cycle.

CRediT authorship contribution statement

Yi Yang: Writing – original draft, Methodology, Investigation, Data curation. **Xianghui Guo:** Writing – review & editing, Writing – original draft, Methodology, Data curation. **Dongjian Ci:** Writing – review & editing, Data curation. **Yi Xu:** Visualization, Data curation. **Yan Li:** Writing – review & editing, Data curation. **Liguo Guo:** Writing – review & editing, Data curation. **Minhan Dai:** Writing – review & editing, Funding acquisition.

Declaration of competing interest

The authors declare that they have no known competing financial interests or personal relationships that could have appeared to influence the work reported in this paper.

Acknowledgement

The crew and scientific staff of the R/V Jiageng, as well as the Joint Chief Scientists of the cruises (Drs. Kuanbo Zhou, Zhimian Cao, Yihua Cai at Xiamen University and Ruifeng Zhang at Shanghai Jiaotong University) are appreciated for their help during the cruises. Yangyang Zhao and Ying Gao collected DIC and TA samples during the spring and summer cruises, respectively. Jiaoyue Ji is appreciated for the helpful discussions about data interpretation. Special thank is to Mr. Xirong Chen at Marine Operations of Xiamen University for taking care of the underway system. This study is supported by the National Natural Science of China through Grant 41890804. Writing of the manuscript was also supported by the Ministry of Science and Technology of China through grant 2022YFF0801402. Rick W. Smith is appreciated for polishing the English.

Appendix A. Supplementary data

Supplementary data to this article can be found online at https://doi.org/10.1016/j.pocean.2025.103515.

Data availability

The data that has been used is confidential.

References

Andersson, A.J., Krug, L.A., Bates, N.R., Doney, S.C., 2013. Sea–air CO_2 flux in the North Atlantic subtropical gyre: Role and influence of Sub-Tropical Mode Water formation. Deep Sea Res. Part II Top. Stud. Oceanogr. 91, 57–70. https://doi.org/10.1016/j.dsr2.2013.02.022.

Ando, K., McPhaden, M.J., 1997. Variability of surface layer hydrography in the tropical Pacific Ocean. J. Geophys. Res. Ocean. 102, 23063–23078. https://doi.org/10.1029/97JC01443.

Ayers, J.M., Lozier, M.S., 2012. Unraveling dynamical controls on the North Pacific carbon sink. J. Geophys. Res. Ocean. 117, C01017. https://doi.org/10.1029/2011JC007368.

Byrne, M.P., Pendergrass, A.G., Rapp, A.D., Wodzicki, K.R., 2018. Response of the Intertropical Convergence Zone to climate Change: Location, Width, and Strength. Curr. Clim. Chang. Reports 4, 355–370. https://doi.org/10.1007/s40641-018-0110-5.

Cai, W.-J., Dai, M., Wang, Y., et al., 2004. The biogeochemistry of inorganic carbon and nutrients in the Pearl River estuary and the adjacent Northern South China Sea. Cont. Shelf Res. 24, 1301–1319. https://doi.org/10.1016/j.csr.2004.04.005.

Cravatte, S., Delcroix, T., Zhang, D., McPhaden, M., Leloup, J., 2009. Observed freshening and warming of the western Pacific Warm Pool. Clim. Dyn. 33, 565–589. https://doi.org/10.1007/s00382-009-0526-7.

Dai, M., Luo, Y.-W., Achterberg, E.P., et al., 2023. Upper Ocean Biogeochemistry of the Oligotrophic North Pacific Subtropical Gyre: from Nutrient sources to Carbon Export. Rev. Geophys. 61. https://doi.org/10.1029/2022RG000800 e2022RG000800.

de Boyer Montégut, C., Madec, G., Fischer, A.S., Lazar, A., Iudicone, D., 2004. Mixed layer depth over the global ocean: an examination of profile data and a profile-based climatology. J. Geophys. Res. Ocean. 109, C12003. https://doi.org/10.1029/2004JC002378.

Dickson, A.G., 1990. Thermodynamics of the dissociation of boric acid in synthetic seawater from 273.15 to 318.15 K. Deep Sea Res. Part a. Oceanogr. Res. Pap. 37, 755–766. https://doi.org/10.1016/0198-0149(90)90004-F.

Dickson, A.G., Sabine, C.L., Christian, J.R., 2007. Guide to best practices for ocean CO_2 measurements. PICES Special Publication.

Dickson, Millero, F.J., 1987. A comparison of the equilibrium constants for the dissociation of carbonic acid in seawater media. Deep Sea Res. Part A. Oceanogr. Res. Pap. 34, 1733–1743. https://doi.org/10.1016/0198-0149(87)90021-5.

Fay, A.R., Gregor, L., Landschützer, P., et al., 2021. SeaFlux: harmonization of air–sea CO_2 fluxes from surface pCO_2 data products using a standardized approach. Earth Syst. Sci. Data 13, 4693–4710. https://doi.org/10.5194/essd-13-4693-2021.

Frierson, D.M.W., Lu, J., Chen, G., 2007. Width of the Hadley cell in simple and comprehensive general circulation models. Geophys. Res. Lett. 34, L18804. https://doi.org/10.1029/2007GL031115.

Gent, P.R., McWilliams, J.C., 1990. Isopycnal mixing in ocean general circulation models. J. Phys. Oceanogr. 20, 150–155. https://doi.org/10.1175/1520-0485(1990)020<0150:IMIOCM>2.0.CO;2.

Gruber, N., Clement, D., Carter, B.R., et al., 2019. The oceanic sink for anthropogenic CO_2 from 1994 to 2007. Science 363, 1193–1199. https://doi.org/10.1126/science.aau5153.

Gruber, N., Gloor, M., Mikaloff Fletcher, S.E., et al., 2009. Oceanic sources, sinks, and transport of atmospheric CO_2. Global Biogeochem. Cycles 23, GB1005. https://doi.org/10.1029/2008GB003349.

Van Heuven, S., D. Pierrot, E. R. Lewis, and D. W. R. Wallace. 2011. MATLAB program developed for CO_2 system calculations ORNL/CDIAC-105b. doi:10.3334/CDIAC/otg.CO2SYS_MATLAB_v1.1.

Iida, Y., Kojima, A., Takatani, Y., Nakano, T., Sugimoto, H., Midorikawa, T., Ishii, M., 2015. Trends in pCO_2 and sea–air CO_2 flux over the global open oceans for the last two decades. J. Oceanogr. 71, 637–661. https://doi.org/10.1007/s10872-015-0306-4.

Iida, Y., Takatani, Y., Kojima, A., Ishii, M., 2021. Global trends of ocean CO_2 sink and ocean acidification: an observation-based reconstruction of surface ocean inorganic carbon variables. J. Oceanogr. 77, 323–358. https://doi.org/10.1007/s10872-020-00571-5.

Ishii, M., Feely, R.A., Rodgers, K.B., et al., 2014. Air–sea CO_2 flux in the Pacific Ocean for the period 1990-2009. Biogeosciences 11, 709–734. https://doi.org/10.5194/bg-11-709-2014.

Ishii, M., Inoue, H.Y., Matsueda, H., et al., 2001. Seasonal variation in total inorganic carbon and its controlling processes in surface waters of the western North Pacific subtropical gyre. Mar. Chem. 75, 17–32. https://doi.org/10.1016/S0304-4203(01)00023-8.

Large, W.G., Pond, S., 1981. Open Ocean Momentum Flux Measurements in Moderate to strong Winds. J. Phys. Oceanogr. 11, 324–336. https://doi.org/10.1175/1520-0485(1981)011<0324:OOMFMI>2.0.CO;2.

Large, W.G., McWilliams, J.C., Doney, S.C., 1994. Oceanic vertical mixing: a review and a model with a nonlocal boundary layer parameterization. Rev. Geophys. 32, 363–403. https://doi.org/10.1029/94RG01872.

Lau, W.K.M., Kim, K.-M., 2015. Robust Hadley Circulation changes and increasing global dryness due to CO_2 warming from CMIP5 model projections. Proc. Natl. Acad. Sci. 112, 3630–3635. https://doi.org/10.1073/pnas.1418682112.

Letscher, R.T., Primeau, F., Moore, J.K., 2016. Nutrient budgets in the subtropical ocean gyres dominated by lateral transport. Nat. Geosci. 9, 815–819. https://doi.org/10.1038/ngeo2812.

Li, Q., Guo, X., Zhai, W., Xu, Y., Dai, M., 2020. Partial pressure of CO_2 and air-sea CO_2 fluxes in the South China Sea: Synthesis of an 18-year dataset. Prog. Oceanogr. 182, 102272. https://doi.org/10.1016/j.pocean.2020.102272.

Li, W., Li, L., Ting, M., Liu, Y., 2012. Intensification of Northern Hemisphere subtropical highs in a warming climate. Nat. Geosci. 5, 830–834. https://doi.org/10.1038/ngeo1590.

Lu, J., Vecchi, G.A., Reichler, T., 2007. Expansion of the Hadley cell under global warming. Geophys. Res. Lett. 34, L06805. https://doi.org/10.1029/2006GL028443.

Mehrbach, C., Culberson, C.H., Hawley, J.E., Pytkowicx, R.M., 1973. Measurement of the apparent dissociation constants of carbonic acid in seawater at atmospheric pressure. Limnol. Oceanogr. 18, 897–907. https://doi.org/10.4319/lo.1973.18.6.0897.

Ogawa, K., Usui, T., Takatani, S., et al., 2006. Shipboard measurements of atmospheric and surface seawater pCO_2 in the North Pacific carried out from January 1999 to October 2000 on the voluntary observation ship MS Alligator Liberty. Pap. Meteorol. Geophys. 57, 37–46. https://doi.org/10.2467/mripapers.57.37.

Oka, E., Qiu, B., 2012. Progress of North Pacific mode water research in the past decade. J. Oceanogr. 68, 5–20. https://doi.org/10.1007/s10872-011-0032-5.

Pierrot, D., Neill, C., Sullivan, K., et al., 2009. Recommendations for autonomous underway pCO_2 measuring systems and data-reduction routines. Deep Sea Res. Part II Top. Stud. Oceanogr. 56, 512–522. https://doi.org/10.1016/j.dsr2.2008.12.005.

Pittman, N.A., Strutton, P.G., Johnson, R., Matear, R.J., Sutton, A.J., 2022. Relationships between Air-Sea CO_2 Flux and New Production in the Equatorial Pacific. Global Biogeochem. Cycles 36, e2021GB007121. https://doi.org/10.1029/2021GB007121.

Qiu, B., Hacker, P., Chen, S., Donohue, K.A., Watts, D.R., Mitsudera, H., Hogg, N.G., Jayne, S.R., 2006. Observations of the Subtropical Mode Water Evolution from the Kuroshio Extension System Study. J. Phys. Oceanogr. 36, 457–473. https://doi.org/10.1175/JPO2849.1.

Le Quéré, C., Andrew, R.M., Friedlingstein, P., et al., 2018. Global Carbon Budget 2018. Earth Syst. Sci. Data 10, 2141–2194. https://doi.org/10.5194/essd-10-2141-2018.

Sabine, C.L., Feely, R.A., Gruber, N., et al., 2004. The Oceanic Sink for Anthropogenic CO_2. Science 305, 367–371. https://doi.org/10.1126/science.1097403.

Sarmiento, J.L., Gruber, N., 2006. Ocean Biogeochemical Dynamics. Princeton Univ. Press.

Seidel, D.J., Fu, Q., Randel, W.J., Reichler, T.J., 2008. Widening of the tropical belt in a changing climate. Nat. Geosci. 1, 21–24. https://doi.org/10.1038/ngeo.2007.38.

Sutton, A.J., Wanninkhof, R., Sabine, C.L., Feely, R.A., Cronin, M.F., Weller, R.A., 2017. Variability and trends in surface seawater pCO_2 and CO_2 flux in the Pacific Ocean. Geophys. Res. Lett. 44, 5627–5636. https://doi.org/10.1002/2017GL073814.

Sweeney, C., Gloor, E., Jacobson, A.R., Key, R.M., McKinley, G., Sarmiento, J.L., Wanninkhof, R., 2007. Constraining global air-sea gas exchange for CO_2 with recent bomb ^{14}C measurements. Global Biogeochem. Cycles 21, GB2015. https://doi.org/10.1029/2006GB002784.

Takahashi, T., Olafsson, J., Goddard, J.G., Chipman, D.W., Sutherland, S.C., 1993. Seasonal variation of CO_2 and nutrients in the high-latitude surface oceans: a comparative study. Global Biogeochem. Cycles 7, 843–878. https://doi.org/10.1029/93GB02263.

Takahashi, T., Sutherland, S.C., Feely, R.A., Cosca, C.E., 2003. Decadal variation of the surface water pCO_2 in the western and central Equatorial Pacific. Science 302, 852–856. https://doi.org/10.1126/science.1088570.

Takahashi, T., Sutherland, S.C., Sweeney, C., et al., 2002. Global sea–air CO_2 flux based on climatological surface ocean pCO_2, and seasonal biological and temperature effects. Deep Sea Res. Part II Top. Stud. Oceanogr. 49, 1601–1622. https://doi.org/10.1016/S0967-0645(02)00003-6.

Takahashi, T., Sutherland, S.C., Wanninkhof, R., et al., 2009. Climatological mean and decadal change in surface ocean pCO_2, and net sea–air CO_2 flux over the global oceans. Deep Sea Res. Part II Top. Stud. Oceanogr. 56, 554–577. https://doi.org/10.1016/j.dsr2.2008.12.009.

Uda, M., Hasunuma, K., 1969. The Eastward Subtropical Countercurrent in the Western North Pacific Ocean. J. Oceanogr. Soc. Japan 25, 201–210. https://doi.org/10.5928/kaiyou1942.25.201.

Wanninkhof, R., Park, G.-H., Takahashi, T., et al., 2013. Global ocean carbon uptake: magnitude, variability and trends. Biogeosciences 10, 1983–2000. https://doi.org/10.5194/bg-10-1983-2013.

Weiss, R.F., 1974. Carbon dioxide in water and seawater: the solubility of a non-ideal gas. Mar. Chem. 2, 203–215. https://doi.org/10.1016/0304-4203(74)90015-2.

Weiss, R.F., Price, B.A., 1980. Nitrous oxide solubility in water and seawater. Mar. Chem. 8, 347–359. https://doi.org/10.1016/0304-4203(80)90024-9.

Williams, R.G., Follows, M.J., 1998. The Ekman transfer of nutrients and maintenance of new production over the North Atlantic. Deep. Res. Part I Oceanogr. Res. Pap. 45, 461–489. https://doi.org/10.1016/S0967-0637(97)00094-0.